Complete prevention of dendrite formation in Zn metal anodes by means of pulsed charging protocols

Grecia Garcia, Edgar Ventosa and Wolfgang Schuhmann**

Analytical Chemistry – Center for Electrochemical Sciences (CES),

Ruhr-Universität Bochum, Universitätstr. 150,

D-44780 Bochum, Germany.

Email: edgar.ventosa@rub.de and wolfgang.schuhmann@rub.de

ABSTRACT

Zn metal as anode in rechargeable batteries such as Zn/air or Zn/Ni batteries suffers from poor cyclability. The formation of Zn dendrites upon cycling is the key limiting step. We report a systematic study of the influence of pulsed electroplating protocols on the formation of Zn dendrites and in turn on strategies to completely prevent Zn dendrite formation. Due to the large number of variables in electroplating protocols, a scanning droplet cell technique was adapted as high-throughput methodology in which a descriptor of the surface roughness can be in-situ derived by means of electrochemical impedance spectroscopy. Upon optimizing the electroplating protocol by controlling nucleation, zincate ion depletion and zincate ion diffusion scanning electron microscopy and atomic force microscopy confirm the growth of uniform and homogenous Zn de-

posits with a complete prevention of dendrite growth. The implementation of pulsed electroplating as charging protocol for commercially available Ni-Zn batteries leads to a substantially prolonged cyclability demonstrating the benefits of pulsed charging in Zn metal based batteries.

KEYWORDS: Zinc, dendrites, batteries, electrodeposition, high-throughput approach.

1. INTRODUCTION

Although the energy density of the state-of-the-art Li-ion batteries (~250 Wh kg^{-1}) is sufficient to fulfil the requirements for hybrid electric vehicles, it is still below the needs for full electric vehicles. [1] Consequently, great efforts have been recently devolved to the development of a new generation of battery systems with significantly higher energy density than that of Li-ion batteries. The use of metal anodes such as metallic lithium, magnesium, aluminum or zinc is seen as a key step in achieving high energy densities. [2,3,4] Among these metal anodes, Zn possesses the most anodic redox potential enabling its use in aqueous medium while the others require organic solvents thus imposing severe safety issues. This fact together with its abundance on earth makes Zn metal anodes based batteries, e.g. Zn/Ni or Zn/air potentially low-cost systems expanding their possible application for stationary energy storage as well. [5,6] However, intrinsic issues of Zn metal anodes, namely hydrogen evolution, dendrite growth and electrode passivation prevent their implementation in commercial rechargeable batteries until now. [4,7,8,9,10]

The dendritic growth upon cycling is the main limitation since it does not only lead to perforation of the separator and short-circuit between positive and negative electrode, but also enhances hydrogen evolution and electrode passivation. A number of strategies have been proposed to address this issue, which can be categorized in four groups. I) The use of special separators between electrodes acting as a physical barrier to prevent short-circuiting. [11] II) Direct modification of the active material. For example, Parker et al. demonstrated that the use of three-dimensional structures of zinc could trap dissolved Zn species such as zincate ions ($Zn(OH)_4^{2-}$) in the vicinity of the electrode upon discharge, thus minimizing redistribution of Zn ions and shape change. [12] III) Electrolyte additives which can be divided into metallic and organic additives. The former include

metallic oxides/hydroxides such as PbO or Bi_2O_3 which are reduced to the metal prior to the reduction of $Zn(OH)_4^{2-}$ ions. [13,14] The metallic film increases the electric conductivity throughout the electrode leading to a more homogeneous current distribution, thus decreasing the shape change. Organic additives such as tetrabutylammonium bromide, [15] tetra-alkyl ammonium hydroxides, [16] triethanolamine, [17] Triton X-100, [18] or polyethylene glycol [19] inhibit dendrite formation by slowing down diffusional mass transport and limiting the enhanced growth at specific sites. IV) Electrochemical approach. In the late 80s and early 90s, there were several studies in which the shape change in Zn metal anodes was proposed to be mitigated by applying direct current (DC) pulses or alternating current (AC) charging protocols. [20,21,22] The reduction of ZnO to Zn metal proceeds via dissolution of $Zn(OH)_4^{2-}$. During the reduction, the concentration of $Zn(OH)_4^{2-}$ is depleted near the electrode surface and the reaction becomes diffusion controlled. Under these conditions, small heterogeneities on the electrode surface trigger the formation of dendrites since sharp features grow faster due to the enhanced mass transport due to the non-planar diffusion (Figure 1) as compared to the planar diffusion and the related mass transport to flat areas.

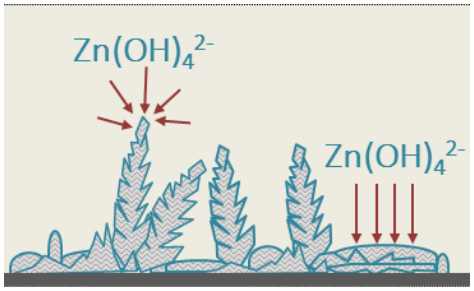


Figure 1. Schematic representation of the diffusion-limited process during Zn electroplating. Planar diffusion at flat surface and planar plus radial diffusion at sharp features.

The application of pulsed DC or AC charging protocols aims at introducing a relaxation time after a short $Zn(OH)_4^{2-}$ reduction to re-establish the concentration of $Zn(OH)_4^{2-}$ at the electrode surface. [23] By this, neighboring sites do not compete for the limited amount of $Zn(OH)_4^{2-}$ under

diffusional mass transport enabling a homogeneous growth at the entire electrode surface. Although interesting results were obtained in the mentioned early studies, the complexity and the large number of interconnected parameters affecting electroplating, e.g. amplitude and duration of the plating pulse, duration of the resting pulse, influence of pre-nucleation pulses, etc. discouraged sustained efforts to achieve a deeper understanding about this electrochemical approach to mitigate dendrite formation.

Although modelling and simulation has shown to be a powerful tool in predicting and accelerating the search for improved charging protocols, [31,32] enormous experimental efforts are still required due to the vast number of variables which has hindered progress especially in pulse charging protocol approach. Herein, we present a high-throughput procedure for the study of pulsed charging protocol for Zn metal anode media using a scanning droplet cell system. This methodology has allowed us to analyze more than 1000 experimental conditions under very reproducible variation of the predominantly influencing parameters of pulse protocols showing the potential of this approach to bridge the gap between modelled and experimental behaviors. Electrochemical impedance spectroscopy (EIS) was employed for deriving a descriptor of the surface roughness in-situ. Optimization of the charging protocol resulted in finding a set of parameters which led to a complete prevention of dendrite formation as confirmed by SEM and AFM measurements.

2. EXPERIMENTAL SECTION

2.1 High-throughput study of Zn electroplating

Metallic zinc was deposited from a solution of 12 M KOH (J. T. Baker, Netherlands) and 1 M $Zn(OH)_4^{2-}$. (ZnO, AnalaR NORMAPUR®, UK) which was prepared using tri-distilled and subsequently deionized water (Millipore, Milli-Q). Zn electroplating was carried out with a scanning droplet cell coupled with a MicroAutolab/FRA potentiostat/galvanostat (Metrohm-Autolab). Note that higher concentration of KOH, 12 M instead of 8 M, were employed to increase and decrease the concentration of zincates and proton, respectively, minimizing the evolution of hydrogen at high current densities. The FRA modulus of the potentiostat was used for in-situ electrochemical impedance spectroscopy measurements at open circuit potential in the frequency range of 50 kHz – 1 Hz. Ag/AgCl 3 M KCl was chosen as reference electrode and a platinum wire of 0.25 µm of diameter as counter electrode. The Teflon tip (head) of the scanning droplet cell had an opening of 1000 µm of diameter (area of 7.85_x10^{-3} cm^2). Glassy carbon and graphite paper (SIGRAFLEX® Folie F02012TH 0,20x500mmx50m) were used as working electrodes. In the case of glassy carbon, it was polished with alumina powder from Buehler (Dusseldorf, Germany), starting from 1.0 µm alpha Al_2O_3, down to 0.3 µm and then 0.05 µm gamma Al_2O_3. Graphite paper was cleaned with ethanol and later the surface was homogenized by polishing with 0.05 µm gamma Al_2O_3. In both cases, cooper tape was stick to the WE to order to ensure proper electrical connection.

2.2 SEM and AFM characterization

The morphology changes of zinc deposits were investigated using a scanning electron microscope (Dual Beam TM 3D FEG; FEI). During the measurements, the chamber was maintained at about $6_x 10^{-10}$ mbar and operating at 20 kV. AFM (NanoWizard 3 from JPK Instruments,) operating in tapping mode in air was used to investigate the topography.

2.3 Evaluation of commercial Zn-Ni batteries

AAA rechargeable Ni-Zn batteries (Powergenix) were tested as received. Galvanostatic chronopotentiometric measurements of commercial Ni-Zn batteries were carried out using a Bio-Logic VMP-3 potentiostat (Bio-Logic). PowerGenix AAA can store 900 mWh, which results in a discharge capacity of 545 mAh for a cell voltage of 1.65 V. Since the best performance of Ni-Zn batteries are achieved at C-rate between 1 – 0.5 C, a charging current of 400 mA was chosen. The voltage range was - 1.2 V / - 2.0 V. CE and RE were short-circuited. The negative side acted as WE while the positive one as CE.

3. RESULTS AND DISCUSSION

3.1 High-throughput study of Zn electroplating

A scanning droplet cell (SDC) was chosen as high-throughput electrochemical technique (Figure 2a) to evaluate a large number of variables within a reasonable timeframe. In short, an electrochemical cell is formed by pressing a Teflon orifice on a current collector to highly reproducibly select a defined electrode area. The selected area is then the working electrode at which any sequence of electrochemical processes can be performed. This type of variable in-situ generated microcell design has been previously used in other fields such as corrosion of materials or photoelectrocatalysts. [24],[25],[26] SDC does not only accelerate the acquisition of experimental data, but also minimizes any human error due to a high degree of automatization of all experiments. Another advantage of this setup is the small area used for each measurement (Figure 2c). Many samples can be prepared on a small area of a current collector hence facilitating fast alternative characterization by microscopy techniques.

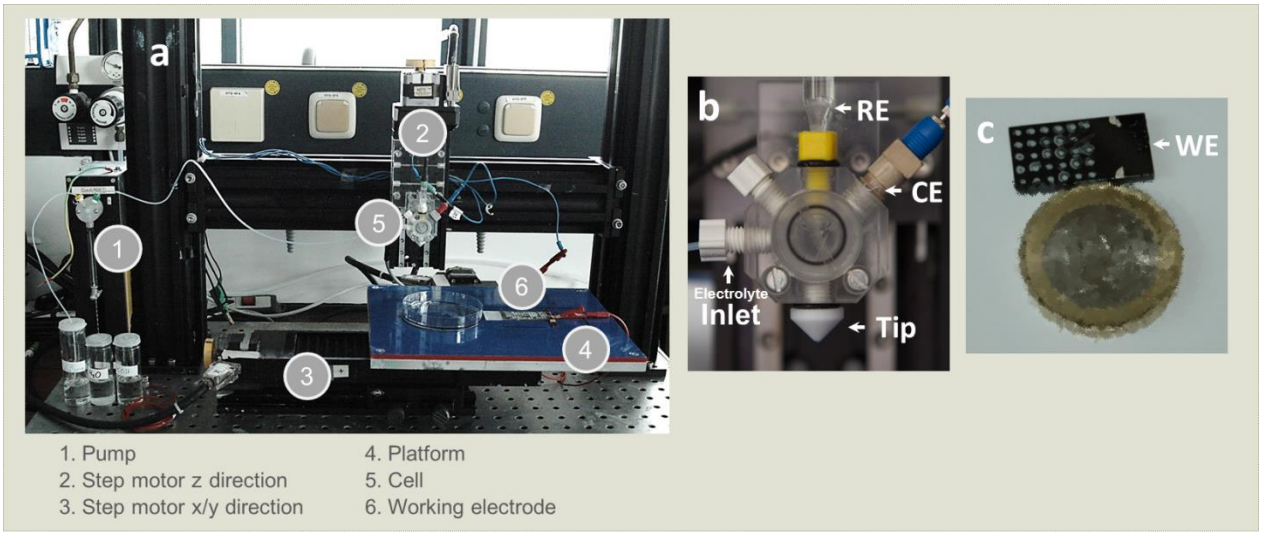


Figure 2. Photograph of a scanning droplet cell system. (a) Entire setup including motors, connections and pump. (1. pump; 2. step motor for the z direction; 3. step motors for x/y-directions; 4. sample platform; 5. electrochemical cell; 6. working electrode) (b) Electrochemical cell (or head) which contains the reference and counter electrode as well as an inlet for pumping the electrolyte. A Teflon tip is located at bottom of the head. The opening of the tip (1 mm in diameter) determines the size of the area of the working electrode. (c) Glassy carbon plate used as working electrode showing 30 small Zn deposits.

Chronoamperometry using a glassy carbon plate as working electrode (Figure 3) showed that the reduction of $Zn(OH)_4^{2-}$ occurs below potentials of -1.60 V (vs. Ag/AgCl/ 3 M KCl) in 12 M KOH containing 1 M $Zn(OH)_4^{2-}$. At low overpotentials, the reaction proceeds under a kinetically-controlled regime. Hence, the concentration of $Zn(OH)_4^{2-}$ at the electrode surface is never completely depleted. The current density increases slightly over time due to the slowly increasing surface area. At high overpotentials, rapid electroplating of Zn leads to a fast increase in surface roughness, which concomitantly leads to a fast increase in current density. The fast consumption

of $Zn(OH)_4^{2-}$ ions depletes their concentration close to the surface leading to a control of the deposition by the diffusion of the zincate ions to the electrode surface. Hence, the time necessary to reach a diffusion-controlled regime depends on the applied overpotential (Figure 3).

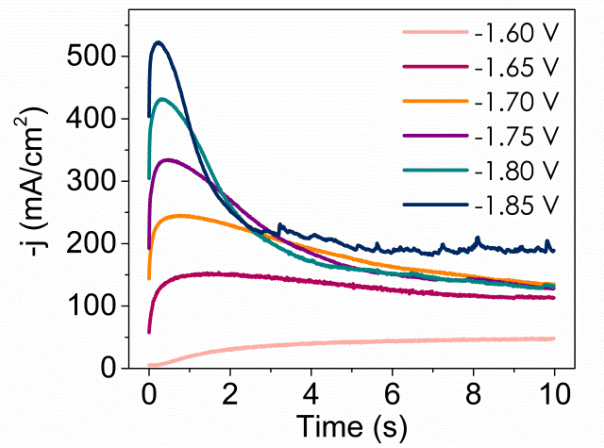


Figure 3. Chronoamperometric current transients for the electrodeposition of Zn onto a glassy carbon plate using a SDC at different applied potentials in 12 M KOH containing 1 M $Zn(OH)_4^{2-}$ ions.

Ideally, the growth of Zn dendrites could be prevented by continuous electroplating establishing a kinetically controlled regime. In this scenario, neighboring sites do not need to compete for zincate ions resulting in a homogeneous film. However, in practice this is not possible due to two reasons. First, electroplating under kinetic control requires the application of small overpotentials or small current densities leading to slow plating rates. Hence, long charging times for a battery would result. Second, reduction of zincate ions occurs outside the stability window of water. Despite the hydrogen evolution reaction (HER) at Zn electrodes is kinetically slow enabling the kinetically faster reduction of the zincate ions, slow charging rates at small current densities enhance the thermodynamically-favored but kinetically-hindered HER. As a result, most of the charge during charging would be consumed by HER instead of the reduction of zincate ions. Therefore, high current densities are desired to avoid parasitic HER and favor the reduction of zincate ions.

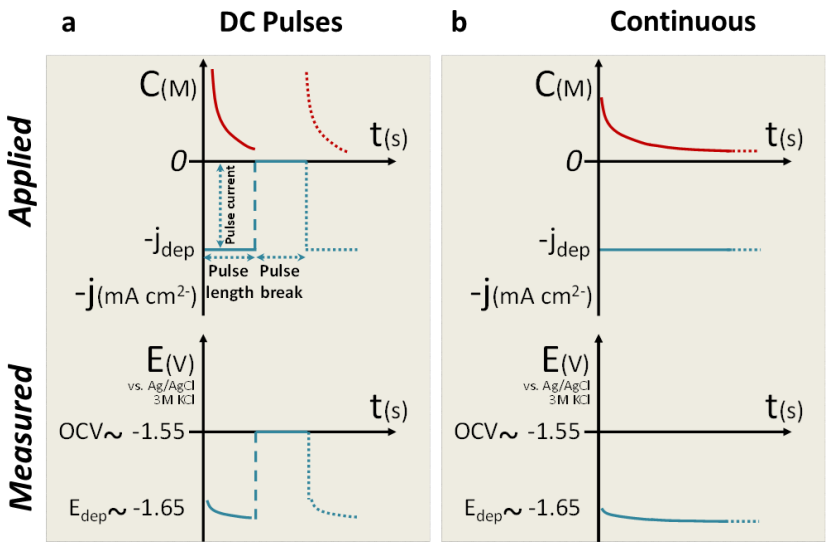


Figure 4. Schematic illustration of Zn electrodeposition by a (a) continuous; (b) a pulsed DC protocol. Potentials are given versus Ag/AgCl/ 3 M KCl.

On the other hand, high current densities result in diffusion-controlled electroplating which in turn promotes formation of Zn dendrites. Since it takes a certain time to reach a diffusion-controlled regime (Figure 3), high current densities may be applied for a short time before complete depletion of zincate ions at the surface takes place. After such a short current pulse at high current densities, the reaction can be stopped in order to allow re-establishing the concentration of zincate ions thus avoiding a diffusion-controlled regime. Consequently, both HER and formation of dendrites could be suppressed by applying short current pulses (Figure 4).

3.2 In-situ roughness evaluation of Zn deposits

Several parameters, such as the amplitude and duration of the electroplating current pulse, the duration of the relaxation pulse or of pre-deposition pulses have to be systematically evaluated. This requires the investigation of a large number of samples (>1000 including replicates), making it practically impossible to analyze the roughness of each of these samples by SEM or AFM within

a reasonable timeframe. We have hence chosen electrochemical impedance spectroscopy (EIS) as a high-throughput electroanalytical method for the in-situ evaluation of the surface roughness after electroplating.

EIS provides information about electrochemical processes occurring at different time constants by applying a sinusoidal perturbation voltage superimposed to a constant applied potential. When the applied frequencies are higher than the time constant of any of the Faraday processes, the overall impedance is dominated by the resistance of the electrolyte and the capacitance of the electrochemical double layer at the electrode interface (Figure 5a). Since the capacitance is directly proportional to the specific capacitance, which is a constant value, and the surface area, it can be used to evaluate changes in the surface area. The capacitance of the electrochemical double layer, CDL, at the electrode interface can be determined by: [27]

$$C_{DL} = -\frac{1}{2\pi f Z_{Im}} \qquad (1)$$

Two simple electroplating conditions were initially chosen to explore the hypothesis. Continuous galvanostatic electroplating at a current density of -50 mA cm^{-2} for 150 s was used as reference sample. The electroplating at -50 mA cm^{-2} was split into 30 pulses with a duration of 5 s inserting a resting and relaxation period of 5 s between two plating pulses. By this, a comparable amount of Zn was deposited in both cases.

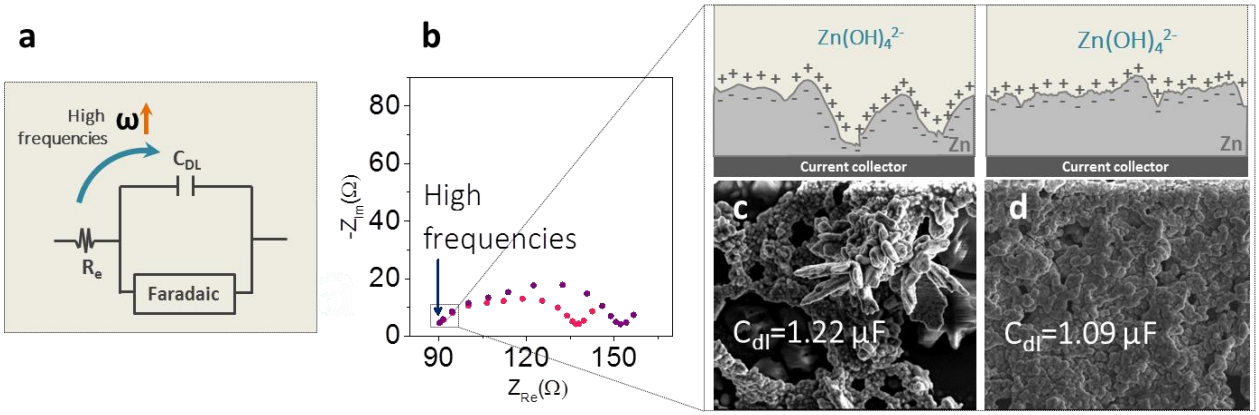


Figure 5. (a) Electric equivalent circuit and (b) Nyquist plot of EIS measurements at Zn films electrodeposited on glassy carbon electrodes. SEM images of Zn films deposited by (c) one continuous pulse of -50 mA cm^{-2} and (d) a pulsed DC protocol (5/5 s, ON/OFF, -50 mA cm^{-2}). The same charge of 7.5 C cm^{-2} was employed for both films. The sketches shown over the SEM images relate the capacitance values measured by EIS with the roughness of the electrode surface. The smoother sample surface, the lower the capacitance value.

SEM images of the two samples clearly show the positive influence of the pulse electroplating. No dendrite formation was observed when applying the pulse protocol (Figure 5c and 5d). EIS was performed at open circuit potential (OCP) immediately after Zn deposition. Figure 5b shows the Nyquist plots of the Zn films. We chose a high frequency (21 kHz) to avoid on the one hand start-up transients and on the other hand small leakage through the Faradaic path (Figure 5a). At 21 kHz, capacitances of 1.22 µF and 1.09 µF for continuous and pulsed electroplating were derived, respectively. The higher capacitance value is due to the higher surface area (Figure 5c and 5d). The same trend was observed at 46 kHz and 10 KHz. In the following, the value of the imaginary part of the impedance at 21 to 24 kHz is used as in-situ derived descriptor of the surface roughness. It should be noted that the imaginary part of the impedance can only be used as an approximate descriptor since both a flat surface with only a few dendrites and a rough surface

without dendrites lead to small values of the capacitance. However, evidently both cases are detrimental for the performance of Zn electrodes. Hence, the primary goal of this work is to find Zn deposition protocols leading to smooth surfaces which exhibit a large imaginary value of the impedance. SEM and AFM were additionally employed for selected samples to evaluate their morphology and by this to confirm the in-situ obtained EIS results.

3.3 Importance of early stages on the deposition of free dendrite Zn electrodes

Graphite paper was used as current collector due to the good adhesion of Zn deposits. As expected, electroplating on graphite paper by means of chronoamperometry at different potentials showed a similar behavior as that on glassy carbon electrodes (see supplementary Figure 1 compared with Figure 3). The diffusion-limited current after 10 s was around -55 mA cm^{-2} for the largest applied overpotentials, a value which is very close to the theoretical one of -60 mA cm^{-2} as predicted by the Cottrell equation. In contrast, on glassy carbon surfaces current densities of about -150 mA cm^{-2} were observed which are attributed to the additional contribution of HER. Obviously, HER is more favorable on glassy carbon surfaces than on graphite paper.

A current density of -56 mA cm^{-2} was chosen for all galvanostatic electroplating experiments since it is a reasonable value for practical battery applications. For example, a Zn electrode with a mass loading of 50 mg cm^{-2} would require a current density of -30 mA cm^{-2} to be charged within 1 h (1 C). As shown above, a simple pulsed electroplating with 5/5 s (ON/OFF) completely prevented Zn dendrite formation (Figure 5c and 5d). For further optimization aiming on even smoother Zn surfaces, pulsed electroplating protocols with shorter pulse duration were investigated. No additional surface smoothing was found by decreasing the electroplating pulse from 5 s to 2 s (Figure 6). Also the duration of the resting period between two subsequent electroplating

pulses did not have a drastic impact on the roughness of the Zn deposits. Interestingly, relaxation periods of 1 s resulted in smoother films as compared to 5 s and 2 s, indicating that a resting time of 1 s between subsequent electroplating pulses is sufficiently long to re-establish the $Zn(OH)_4^{2-}$ ion concentration at the electrode surface.

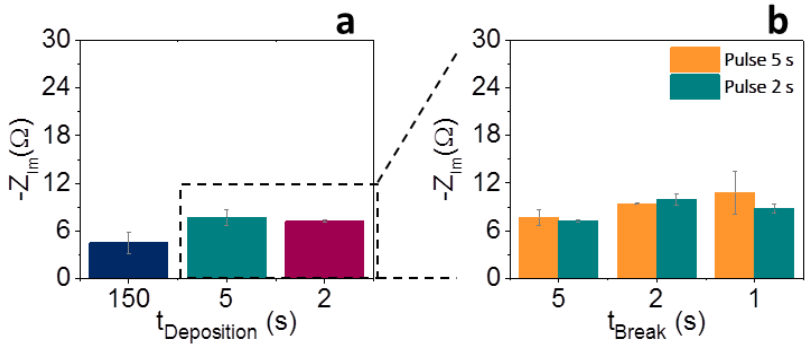


Figure 6. Imaginary part of impedance, $-Z_{Im}$, at a frequency of ~24 kHz for Zn films deposited at different conditions. (a) Influence of the duration of the electroplating pulse (2 s relaxation break). (b) Influence of the duration of the relaxation break. A current density of -56 mA cm^{-2} and a total charge of 8.4 C cm^{-2} were applied to all samples. (n > 10).

In order to further decrease the roughness of the deposited Zn films, an additional step was implemented into the charging protocol. From studies on nucleation and growth of metals it is known that the early stages of the electrochemical deposition are of high importance for the further growth of the metal deposit. [28]. The number of active sites at which nuclei grow increases with increasing overpotential. In order to achieve a high coverage of Zn, which prevents HER and the creation of a few preferential metal deposition sites leading in turn to the growth of dendrites, a short current pulse with a high current density and concomitantly a high overpotential was implemented at the beginning of the charging protocol (Figure 7a). After the initial short and high amplitude electroplating pulse which is essentially a nucleation pulse, the charging protocol was continued with current pulses of lower amplitude (-56 mA cm^{-2}).

The influence of the duration and amplitude of the nucleation pulse, which is applied only once at the beginning of the charging protocol, on the roughness of the deposited Zn film was evaluated using in-situ EIS. The results are summarized in figures 7b, 7c, 7d and 7e and correspond to the influence of the nucleation pulse on the subsequent 5/2, 5/1, 2/2 and 2/1 s (ON/OFF) pulsed DC protocol, respectively. The highest value of the imaginary part in the corresponding in-situ EIS ($-Z_{Im}$ = 24.7±1.9 Ω) was achieved for a nucleation pulse with a duration and amplitude of 1 s and -168 mA cm^{-2}, respectively, followed by a 2/1 s (ON/OFF) pulsed DC protocol with an amplitude of -56 mA cm^{-2}. The implementation of a short nucleation pulse applied only once at the beginning of the pulsed DC charging protocol (2/1, ON/OFF) led to a 3-fold decrease in the average roughness and a 5.5 fold decrease as compared to continuous electroplating without any relaxation periods

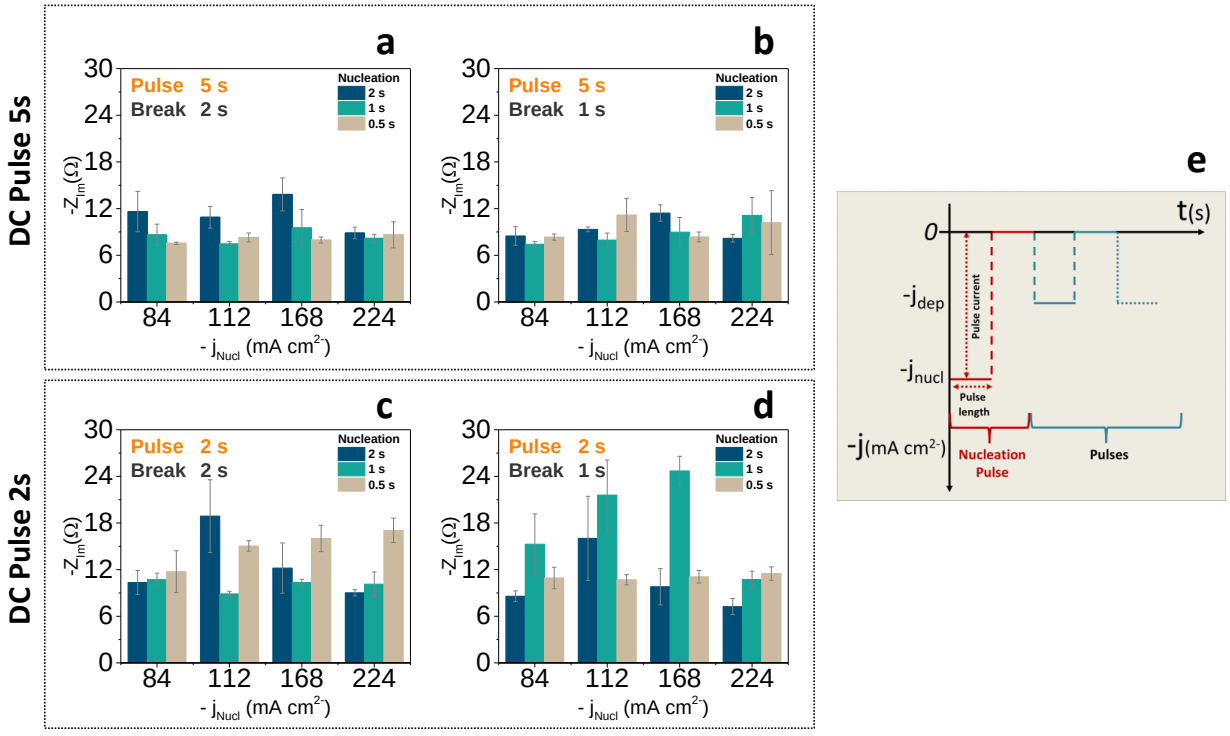


Figure 7. Imaginary part of the impedance, $-Z_{Im}$, at a frequency of ~24 kHz at Zn films obtained at different electroplating conditions. The nucleation step is applied only once before the pulsed

charging protocol. A nucleation step of -84, -112, -168 and -224 mA cm^{-2} for 0.5, 1 or 2 s followed by a pulsed DC charging protocol of -56 mA cm^{-2}: 5/2 s, 5/1 s, 2/2 s and 2/1 s (ON/OFF) for (a), (b), (c) and (d), respectively. The same charge (8.4 C cm^{-2}) was consumed for the electrodeposition of all films. A table giving detailed information about the measurements is included in the supplementary information. (e) Schematic representation of a nucleation step followed by the pulsed DC charging protocol. (n>5).

3.4 Scanning electron microscopy and atomic force microscopy

Since the roughness values as obtained from EIS data are only approximate descriptors, SEM and AFM at selected samples were used to validate the results of the high-throughput in-situ EIS measurements. Three samples were selected namely one obtained by continuous electroplating, one from a 2/1 s (ON/OFF) pulsed DC protocol (-56 mA cm^{-2}), and one with an additional nucleation pulse (1 s at -168 mA cm^{-2}) followed by the 2/1 s (ON/OFF) pulsed DC protocol (-56 mA cm^{-2}). The SEM results were consistent with the EIS data (Figure 8). Dendrites were clearly visible for the sample obtained by continuous electroplating. The formation of dendrites was largely prevented by applying a 2/1 s (ON/OFF) pulsed DC protocol. However, the electrode surface was not completely uniform as discontinuities in the Zn film such as empty gaps could be observed. Introducing a short nucleation pulse at higher current density before the 2/1 s (ON/OFF) pulsed DC protocol led to an apparently smoother film without any visible discontinuities.

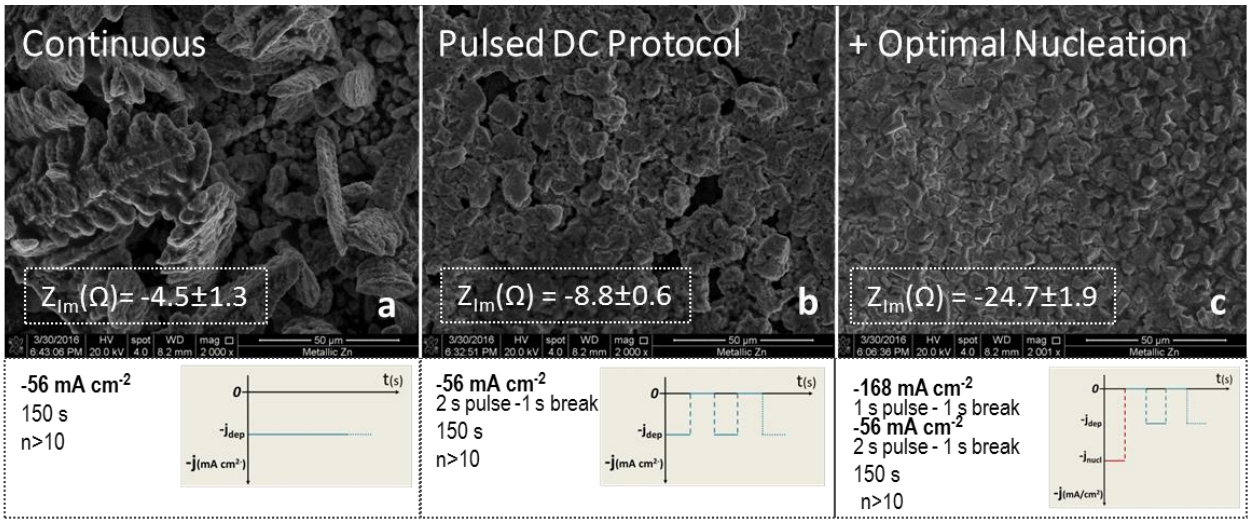


Figure 8. SEM images of Zn films electrodeposited on graphite paper from a solution of 12 M KOH containing 1 M $Zn(OH)_4^{2-}$ by applying (a) one continuous charging pulse of 150 s at -56 mA cm^{-2}, (b) a pulsed DC (2/1 s, ON/OFF, -56 mA cm^{-2}) protocol and (c) a nucleation step at -168 mA cm^{-2} for 1 s followed by a pulsed DC (2/1 s, ON/OFF, -56 mA cm^{-2}) protocol. The electrodeposition conditions are given and are schematically illustrated below each SEM image. The value of $-Z_{Im}$ from EIS is also provided. (n>10).

Since SEM shows only a two-dimensional representation of the morphology, AFM was additionally employed to provide the required three-dimensional information and thus to confirm the benefits of the nucleation pulse for achieving smooth Zn deposits. AFM measurements were also attempted on continuous electroplated Zn films, however, due to the presence of dendrites the roughness of these samples exceeded the limits of our AFM (max. z-height of 8 µm). Figure 9 shows AFM images of the films deposited using pulsed DC protocols with and without nucleation pulse. AFM measurements confirmed that introducing a short nucleation step resulted in smoother films in addition to preventing discontinuities in the film (Figure 8).

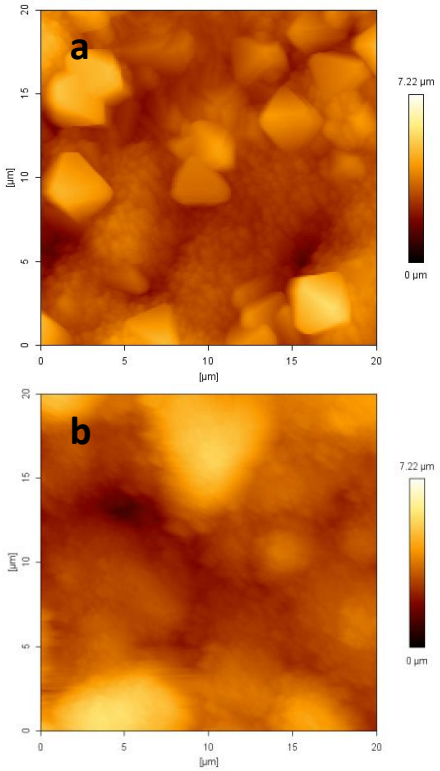


Figure 9. AFM images of Zn films deposited on graphite paper from a solution of 12 M KOH containing 1 M $Zn(OH)_4^{2-}$ ions by applying (a) pulsed DC protocol (2/1 s, ON/OFF, at -56 mA cm^{-2}) and (b) an initial nucleation step (1 s at -168 mA cm^{-2}) followed by the pulsed DC protocol (2/1 s, ON/OFF, at -56 mA cm^{-2}).

3:5 Influence of the pulsed DC charging protocol on commercial rechargeable Ni-Zn batteries

The previous results demonstrate that the formation of dendrites and roughening of the electrode surface during charging can be prevented by applying pulsed DC protocols comprising relaxation periods between short electroplating pulses. Since preventing dendrite formation at Zn electrodes should be beneficial for the long-term performance and especially for the cyclability of Ni-Zn batteries, commercially available AAA Ni-Zn batteries from PowerGenix (Figure 10a) were purchased and used to explore the impact of a pulsed DC charging protocol on their cyclability.

The commercial AAA Ni-Zn batteries can store 900 mWh, which results in a discharge capacity of 545 mAh at a cell voltage of 1.65 V.

Since AAA Ni-Zn batteries are recommended by the manufacturer to be charged at a C-rate bet-ween 1 to 0.5 C, a charging current of 400 mA was chosen. It should be noted that all given voltage values are positive because the Ni electrode is connected as the working electrode. The voltage range was -2.0 / -1.2 V, except for the first cycle in which the upper cut-off was increased to -2.2 V (see voltage profiles in the supplementary information). This was necessary due to the phase transformation at the Ni electrode during the first cycle. [29] Oxygen evolution at the Ni electrode during the first cycle was responsible for the observed lower coulombic efficiency in this cycle (see supplementary Figure 3). [30] Figure 10b shows the charge capacity obtained from a commercial Ni-Zn battery when applying continuous, and pulsed DC (5/2 s, ON/OFF) and pulsed DC (2/1 s, ON/OFF) charging protocols (without nucleation step).

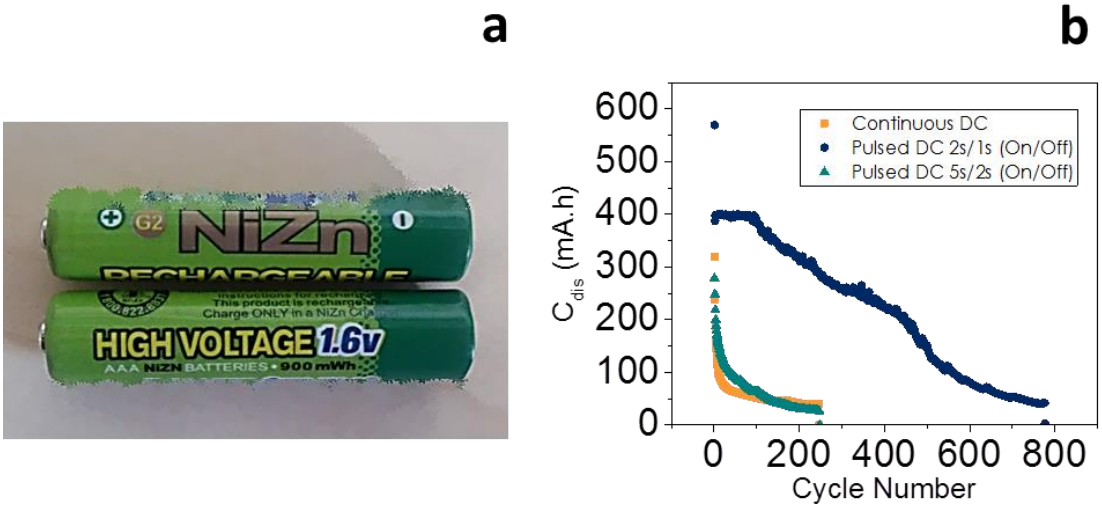


Figure 10. (a) Photograph of two commercial Ni-Zn AAA batteries from PowerGenix. (b) Discharge capacity of PowerGenix AAA Ni-Zn batterFigies charged using continuous (orange) and

pulsed-DC protocols: (2/1 s, ON/OFF) (blue), (5/2 s, ON/OFF) (turquoise) protocol at a current of 400 mA (nucleation step was not applied).

For continuous charging, the discharge capacity rapidly dropped below 25% of the theoretical value (136 mAh) during the first 10 cycles. It should be noted that several new batteries were tested all delivering similar performances. When applying the pulsed DC (2/1 s, ON/OFF) charging protocol, the discharge capacity remained above 50 % (272 mAh) and 25 % (136 mAh) of the theoretical value for 275 cycles and >500 cycles, respectively. These results clearly demonstrate that the prevention of dendrite formation and the electroplating of smoother Zn films achieved by pulsed DC charging protocols lead to improved performances even for commercial batteries based on Zn anodes. On the other hand, no improvement was observed when applying the pulsed DC (5/2 s, ON/OFF) charging protocol due to the fact that the duration of the pulse (5 s) was too long. The lack of improvement for this pulsed DC protocol clearly shows the importance of optimizing the charging protocol for the commercial device.

4. CONCLUSIONS

The formation of undesired Zn dendrites during electroplating under diffusion-controlled regime occurs due to the enhanced mass transport at sharp features with respect to flat surfaces. The introduction of short resting periods during the electroplating of Zn prevents the formation of Zn dendrites resulting in smoother films since the concentration of zincates is re-established at the electrode surfaces avoiding the competition of neighbouring sites for zincates.

Scanning droplet cell containing a solution of in 12 M KOH + 1 M $Zn(OH)_4^{2-}$ allows exploring many different pulsed DC protocol in order to find optimal Zn electroplating conditions. The introduction of a nucleation pulse (short pulse of large amplitude), which allows achieving high initial coverage of Zn nuclei, appears to be more important than the length and the plating and resting pulses. The combination of optimal nucleation step and pulsed DC charging protocol results in smooth Zn films, preventing completely the formation of dendrites and discontinuities in the film.

Commercially available Ni-Zn batteries such as PowerGenix AAA (900 mWh) benefit from pulsed DC charging protocols. The cyclability of a PowerGenix battery can be prolonged from few dozen of cycles to several hundreds of cycles when (dis)charged at 400 mAh. Therefore, the insights gathered for Zn electroplating using a model system are valid for commercial Zn anode based batteries.

Supporting Information: Table showing the record of the imaginary part of impedance, $-Z_{Im}$, at a frequency of ~24 kHz at Zn film obtained at different electroplating conditions. Figure corresponding to the potentiostatic current density transients for the deposition of Zn in graphite paper. Two figures showing the Charge-Discharge curves for the galvanostatic cycling with potential limitation of Ni-Zn PowerGenix AAA cells.

Corresponding Author

*Prof. Wolfgang Schuhmann, e-mail: wolfgang.schuhmann@rub.de, tel: +49 234 32 26200

*Dr. Edgar Ventosa, e-mail: edgar.ventosa@rub.de, tel: +49 234 32 25474

ACKNOWLEDGMENT

Financial support from the Helmholtz Association through the "Initiative and Networking Fund" in the framework of the Helmholtz Energie Allianz "Stationäre elektrochemische Feststoffspeicher und -wandler" (HA-E-0002) is gratefully acknowledged. G.G is grateful for a PhD scholarship from the International Max-Planck Research School for Surface and Interface Engineering in Advanced Materials (IMPRS-SurMat).

REFERENCES

(1) Wagner, F. T.; Lakshmanan, B.; Mathias, M. F. Electrochemistry and the Future of the Automobile. *J. Phys. Chem. Lett.* 2010, *1*, 2204–2219, DOI: 10.1021/jz100553m.

(2) Elia, G. A.; Marquardt, K.; Hoeppner, K.; Fantini, S.; Lin, R.; Knipping, E.; Peters, W.; Drillet, J.-F.; Passerini, S.; Hahn, R. An Overview and Future Perspectives of Aluminum Batteries. *Adv. Mater.* **2016**, *28*, 7564–7579, DOI: 10.1002/adma.201601357.

(3) Armand, M.; Tarascon, J.-M. Building Better Batteries. *Nature.* **2008**, *451*, 652–657, DOI: 10.1038/451652a.

(4) Kim, H.; Jeong, G.; Kim, Y.-U.; Kim, J.-H.; Park, C.-M.; Sohn, H.-J. Metallic Anodes for Next Generation Secondary Batteries. *Chem. Soc. Rev.* **2013**, *42*, 9011–9034, DOI: 10.1039/c3cs60177c.

(5) Lee, J.-S.; Tai Kim, S.; Cao, R.; Choi, N.-S.; Liu, M.; Lee, K. T.; Cho, J. Metal-Air Batteries with High Energy Density: Li-Air versus Zn-Air. *Adv. Energy Mater.* **2011**, *1*, 34–50, DOI: 10.1002/aenm.201000010.

(6) Li, Y.; Dai, H. Recent Advances in Zinc-Air Batteries. *Chem. Soc. Rev.* **2014**, *43*, 5257–5275, DOI: 10.1039/c4cs00015c.

(7) Mainar, A.R.; Leonet, O.; Bengoechea, M.; Boyano I.; de Meatza1, I;.Kvasha, A.; Guerfi, A.; Blázquez, J.A. Alkaline Aqueous Electrolytes for Secondary Zinc–Air Batteries: an Overview. *Int. J. Energy Res.* **2016**, *40*, 1032–1049. DOI: 10.1002/er.3499.

(8) Gallaway, J.; Gaikwad, A.; Hertzberg, B.; Erdonmez, C.; Chen-Wiegart, Y.; Sviridov, L.; Evans-Lutterodt, K.; Wang, J.; Banerjee, S.; Steingart, D. An In Situ Synchrotron Study of Zinc Anode Planarization by a Bismuth Additive. *J. Electrochem. Soc*. **2014**, *161*, A275-A284. DOI: 10.1149/2.037403jes

(9) Davies, G.; Hsieh, A.; Hultmark, M.; Mueller, M.; Steingart, D. Utilization of Hyper-Dendritic Zinc during High Rate Discharge in Alkaline Electrolytes. *J. Electrochem. Soc.* **2016**, *163*, A1340-A1347. DOI: 10.1149/2.0891607jes

(10) Li, J.; Zhao, T.; Shangguan, E.; Li, Y.; Li, L.; Wang, D. Wang, M.; Chang, Z.; Li, Q. Enhancing the Rate and Cycling Performance of Spherical ZnO Anode Material for Advanced Zinc-Nickel Secondary Batteries by Combined In-Situ Doping and Coating with Carbon. *Electrochim. Acta* **2017**, *236*, 180–189. DOI: 10.1016/j.electacta.2017.03.164

(11) Kritzer, P.; Cook, J. A. Nonwovens as Separators for Alkaline Batteries. *J. Electrochem. Soc.* **2007**, *154*, A481-A494, DOI: 10.1149/1.2711064.

(12) Parker, J. F.; Chervin, C. N.; Nelson, E. S.; Rolison, D. R.; Long, J. W. Wiring Zinc in Three Dimensions Re-Writes Battery Performance-Dendrite-Free Cycling. *Energy Environ. Sci.* **2014**, *7*, 1117-1124, DOI: 10.1039/c3ee43754j.

(13) McBreen, J.; Gannon, E. The Electrochemistry of Metal Oxide Additives in Pasted Zinc Electrodes. *Electrochim. Acta* **1981**, *26*, 1439–1446, DOI: 10.1016/0013-4686(81)90015-3.

(14) McBreen, J.; Gannon, E. Bismuth Oxide as an Additive in Pasted Zinc Electrodes. *J. Power Sources* **1985**, *15*, 169–177, DOI: 10.1016/0378-7753(85)80070-7.

(15) Wang, J. M.; Zhang, L.; Zhang, C.; Zhang, J. Q. Effects of Bismuth Ion and Tetrabutylammonium Bromide on the Dendritic Growth of Zinc in Alkaline Zincate Solutions. *J. Power Sources* **2001**, *102*, 139–143, DOI: 10.1016/S0378-7753(01)00789-3.

(16) Lan, C. J.; Lee, C. Y.; Chin, T. S. Tetra-Alkyl Ammonium Hydroxides as Inhibitors of Zn Dendrite in Zn-Based Secondary Batteries. *Electrochim. Acta* **2007**, *52*, 5407–5416, DOI: 10.1016/j.electacta.2007.02.063.

(17) Sharma, Y.; Aziz, M.; Yusof, J.; Kordesch, K. Triethanolamine as an Additive to the Anode to Improve the Rechargeability of Alkaline Manganese Dioxide Batteries. *J. Power Sources* **2001**, *94*, 129–131, DOI: 10.1016/S0378-7753(00)00633-9.

(18) Kan, J.; Xue, H.; Mu, S. Effect of Inhibitors on Zn-Dendrite Formation for Zinc-Polyaniline Secondary Battery. *J. Power Sources* **1998**, *74*, 113–116, DOI: 10.1016/S0378-7753(98)00040-8.

(19) Banik, S. J.; Akolkar, R. Suppressing Dendrite Growth during Zinc Electrodeposition by PEG-200 Additive. J. *Electrochemic. Soc.* **2013**, *160*, D519-D523, DOI: 10.1149/2.040311jes.

(20) Arouete, S.; Blurton, K. F.; Oswin, H. G. Controlled Current Deposition of Zinc from Alkaline Solution. *J. Electrochem. Soc.* **1969**, *116*, 166-169, DOI: 10.1149/1.2411787.

(21) McBreen, J. Zinc Electrode Morphology in Alkaline Solutions. *J. Electrochem. Soc.* **1983**, *130*, 1641-1645, DOI: 10.1149/1.2120055.

(22) Katz, M. H.; Adler, T. C.; McLarnon, F. R.; Cairns, E. J. The Effect of Pulse Charging on the Cycle-Life Performance of Zinc/Nickel Oxide Cells. *J. Power Sources* **1988**, *22*, 77–95, DOI: 10.1016/0378-7753(88)80007-7.

(23) Thirsk, H. R. *Electrochemistry: Volume 4,* Ed.; The Royal Society of Chemistry, Burlington House, London, 1974.

(24) Youssef, K. M.; Koch, C. C.; Fedkiw, P. S. Influence of Pulse Plating Parameters on the Synthesis and Preferred Orientation of Nanocrystalline Zinc from Zinc Sulfate Electrolytes. *Electrochim. Acta* **2008**, *54*, 677–683, DOI: 10.1016/j.electacta.2008.07.048.

(25) Hassel, A. W.; Lohrengel, M. M. The Scanning Droplet Cell and its Application to Structured Nanometer Oxide Films on Aluminium. *Electrochim. Acta* **1997**, *42*, 3327–3333, DOI: 10.1016/S0013-4686(97)00184-9.

(26) Lohrengel, M. M. Interface and Volume Effects in Biological Cells and Electrochemical Microcells. *Electrochim. Acta* **1997**, *42*, 3265–3271, DOI: 10.1016/S0013-4686(97)00177-1.

(27) Barsoukov, E.; Macdonald, J. R. *Impedance Spectroscopy: Theory, Experiment, and Applications*, Second Ed.; Wiley-Interscience, a John Wiley & Sons, Inc., publication: Hoboken, New Jersey, 2005.

(28) Penner, R. M. Brownian Dynamics Simulations of the Growth of Metal Nanocrystal Ensembles on Electrode Surfaces in Solution: 2. The Effect of Deposition Rate on Particle Size Dispersion †. *J. Phys. Chem. B.* **2001**, *105*, 8672–8678, DOI: 10.1021/jp0112828.

(29) Tuomi, D. The Forming Process in Nickel Positive Electrodes. *J. Electrochem. Soc.* **1965**, *112*, 1, DOI: 10.1149/1.2423457.

(30) Garcia, G.; Schuhmann, W.; Ventosa, E. A Three-Electrode, Battery-Type Swagelok Cell for the Evaluation of Secondary Alkaline Batteries: The Case of the Ni-Zn Battery. *ChemElectroChem.* **2016**, *3*, 592–597, DOI: 10.1002/celc.201500474.

(31) Wang, K.; Pei, P.; Ma, Z.; Chen, H.; Xu, H.; Chen, D.; Wang, X. Dendrite Growth in the Recharging Process of Zinc–Air Batteries. *J. Mater. Chem. A* **2015**, *3*, 22648–22655, DOI: 10.1039/C5TA06366C.

(32) Wang, K.; Pei, P.; Ma, Z.; Xu, H.; Li, P.; Wang, X. Morphology Control of Zinc Regeneration for Zinc–Air Fuel Cell and Battery. *J. Power Sources*. **2014**, *271*, 65–75. DOI: 10.1016/j.jpowsour.2014.07.182.

Table of Contents/Abstract Graphic

